Technical Sciences, 2017, 20(3), 289–296

Quarterly peer-reviewed scientific journal
ISSN 1505-4675
e-ISSN 2083-4527
TECHNICAL SCIENCES
Homepage: www.uwm.edu.pl/techsci/

CHANGES OF CRYSTALLITE SIZES IN THE OXIDE LAYER FORMING DURING LONG-TERM OPERATION OF 10CrMo9-10 STEEL

Monika Gwoździk

Institute of Materials Engineering
Faculty of Production Engineering and Materials Technology
Czestochowa University of Technology

Received 26 January 2016, accepted 14 April 2017, available online 4 May 2017.

K e y w o r d s: 10CrMo9-10 steel, oxide layer, X-ray diffraction, crystallite sizes.

A b s t r a c t

The paper contains results of the studies on X-ray diffraction analysis XRD (studying the phase composition, crystallite sizes) of oxide layers on 10CrMo9-10 steel, operated for a long time at an elevated temperature (T = 525°C, t = 200,000 h). The oxide layer was studied on a surface and a cross-section at the outer on the inlet both on the fire and counter-fire side of the tube wall surface. X-ray studies were carried out on the outer surface of a tube, and then the layer surface was polished down and the diffraction measurements were performed again to determine crystallite size in oxide layers. Based on the width and the position of the main coat and substrate reflections, the size of the crystallites was determined using the Scherrer formula.

Introduction

Currently, many scientific centres are conducting diversified materials research related to surface engineering (FRANGINI et al. 2014, LABISZ 2014, 2015, ŢĂLU et al. 2015, KULESZA, BRAMOWICZ 2014, SZAFARSKA, IWASZKO 2012), particularly with the oxidation of steel used in the power industry (BISCHOFF et al. 2013, PRISS et al. 2014, ANTONOV et al. 2013).

Correspondence: Monika Gwoździk, Instytut Inżynierii Materiałowej, Politechnika Częstochowska, ul. Armii Krajowej 19, 42-200 Częstochowa, e-mail: gwozdzik.monika@wip.pcz.pl

In the power industry, apart from low-alloy steels like 10CrMo9-10 (10H2M) or 13CrMo4-5 (15HM), also high-alloy steels are used, such as e.g. X10CrMoVNb9-1 (P91), which is characterised primarily by an increased chromium content. A higher chromium content makes that this steel has better anti-corrosion properties as compared with low-alloy steels. However, despite that there is a need to diagnose both this steel and low-alloys steels resistance to the operation of a steam and flue gases environment existing in components operated long time at high temperatures and during a few hundred thousand hours (GWOŹDZIK 2014, 2016, KLEPACKI, WYWROT 2010, KLEPACKI 2006).

Studies carried out have shown that the kinetics of corrosion on steels operating long-term at elevated temperatures is complex and depends inter alia on (GWOŹDZIK 2014): chemical composition of steel, operating temperature of the element, operating time, flowing medium (flue gas side, steam side), flue gas type, morphology of individual oxide layers.

In paper (GWOŹDZIK 2013) it has been found that $NaFePO_4$, $Zn_2P_2O_7$, Na_2SO_4, $Fe_3(PO_4)_2$, Al_2SiO_5, $ZnSO_4$ are formed as a result of long-term operation (t = 100,000 h) of 10CrMo9-10 steel at the temperature of 575°C (directly from the exhaust gas). Hematite (Fe_2O_3) occurs on the outer surface of the tube. Then magnetite (Fe_3O_4) appears below hematite.

Material and Experimental Methods

The material studied comprised specimens of 10CrMo9-10 steel taken from a pipeline operated at the temperature of 525°C during 200,000 hours. The oxide layer was studied on a surface and a cross-section at the outer on the inlet both on the fire and opposite fire (counter-fire) side of the tube wall surface Figure 1.

Thorough examinations of the oxide layer carried out on the outer surface of tube wall comprised:

– microscopic examinations of the oxide layer were performed using an Olympus SZ61 and GX41 optical microscope (LM), Jeol JSM-6610LV scanning electron microscope (SEM),

– thickness measurements of formed oxide layers,

– chemical composition analysis of deposits/oxides using a Jeol JSM-6610LV scanning electron microscope (SEM) working with an Oxford EDS electron microprobe X-ray analyser,

– X-ray (XRD) measurements (studying the phase composition, crystallite sizes); the layer was subject to measurements using a Seifert 3003T/T X-ray diffractometer and the radiation originating from a tube with a cobalt anode

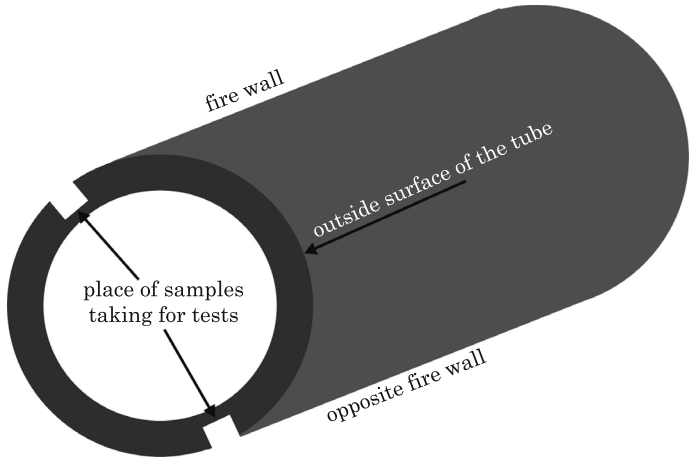

Fig. 1. Place of samples taking for tests

(λ_{Co} = 0.17902 nm). X-ray studies were performed, comprising measurements in a symmetric Bragg-Brentano geometry (XRD). A computer software and the DHN PDS, PDF4+2009 crystallographic database were used for the phase identification. X-ray studies were carried out on the outer surface of a tube, and then the layer surface was polished down and the diffraction measurements were performed again to determine individual oxide layers.

The size of crystallites of oxides was determined by the Scherrer relationship. Methods based on the analysis of diffraction line profile are used to determine the size of crystallites smaller than 100 nm and of lattice deformations (GWOŹDZIK 2016). Based on the width and the position of the main coat and substrate reflections, the size of the crystallites was determined using the Scherrer formula (1):

$$D_{hkl} = \frac{\mathrm{k} \cdot \lambda}{\beta \cdot \cos\Theta} \tag{1}$$

where:
D_{hkl} – crystallite size in the direction normal to (hkl) [nm],
k – constant (~1);
λ – radiation wavelength [nm],
β – reflection width depending on the crystallite size [rad],
Θ – Bragg angle [rad].

Results of examinations

The obtained results of macroscopic and microscopic studies on the oxides/deposits layer surface (Fig. 2) have shown a much greater degree of surface development on the fire side than on the counter-fire side. In addition, SEM studies (Figs. 2*c*, *d*) have shown that the formed deposits layer in certain places has a spheroidal nature. As compared with the counter-fire side the deposits formed on the fire side have larger dimensions.

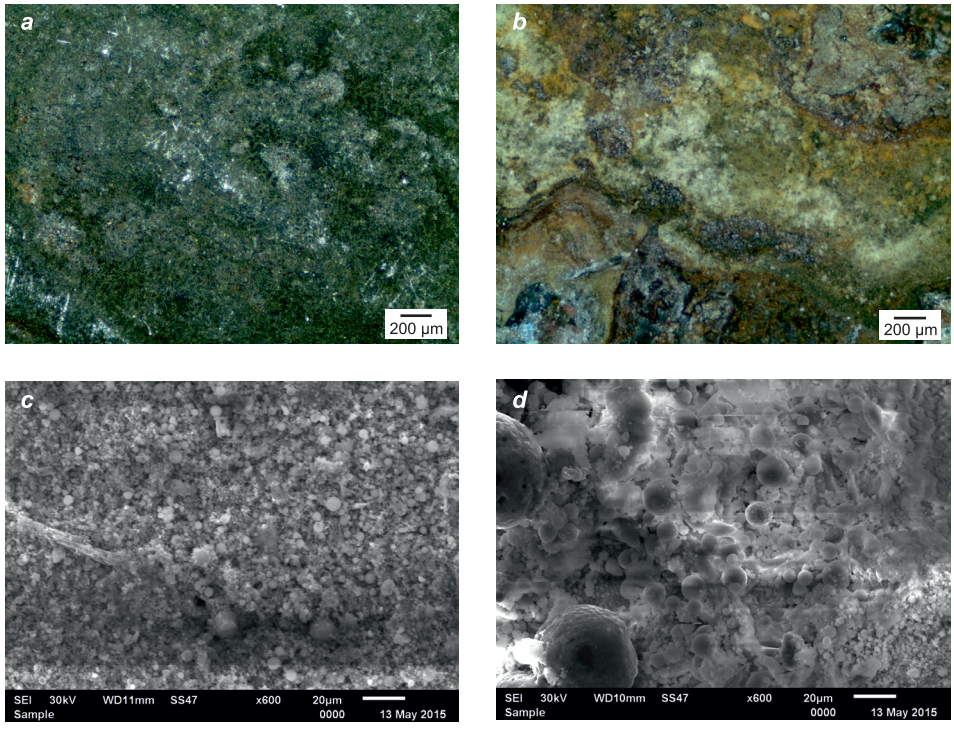

Fig. 2. Oxides formed on 10CrMo9-10 steel operated at 525°C during 200,000 hours: *a* – opposite fire wall LM (light microscopy), *b* – fire wall LM, *c* – opposite fire wall SEM (scanning electron microscopy), *d* – fire wall SEM

Microscopic examinations carried out on transverse microsections (Fig. 3) have shown that the deposits formed on the counter-fire side had a small thickness, reaching the depth of 9,83 µm. Instead, the formed oxide layer is 78.01 µm thick. On the fire side the deposits are 539 µm thick, while oxides 182,71 µm. The formed oxides/deposits layer, especially on the flue gas inflow side, is damaged to a significant extent.

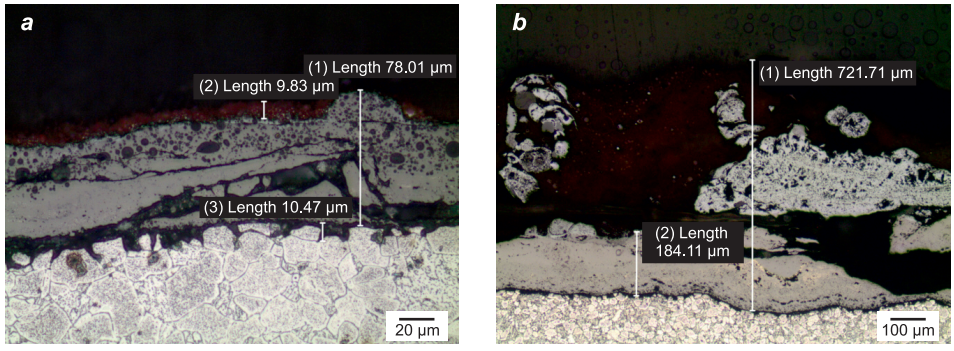

Fig. 3. The thickness of oxides layer formed on the steel examined: *a* – opposite fire wall – LM, *b* – fire wall – LM

The chemical analysis (EDS) (Fig. 4) comparison with XRD analysis on the fire side have shown that on the outside there are such deposits as: $CaSiO_2$, Al_2SiO_5 and $CaSO_4$. Fe_2O_3 and Fe_3O_4 oxides exist under this layer. Similar oxides were observed on the counter-fire side.

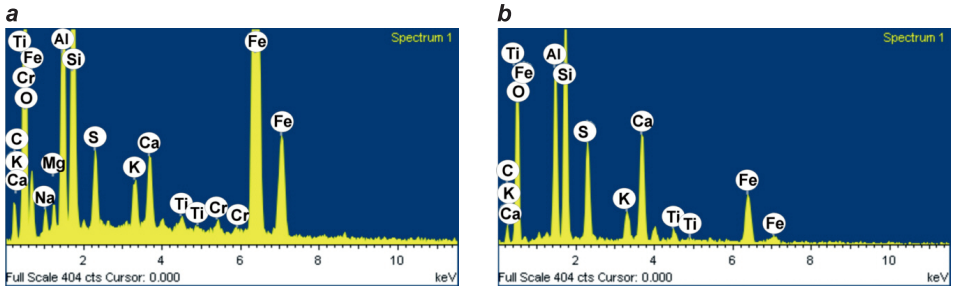

Fig. 4. EDS point microanalysis: *a* – opposite fire wall, *b* – fire wall

The size of Fe_2O_3 crystallites was determined for the (104) plane, while for Fe_3O_4 for the (311) plane. A layers of oxide 78 µm and 200 µm thick were studied (after polishing deposits), then the surface of the formed layer was polished in 11, 11, 9 and 15 cycles for Fe_2O_3 – opposite fire wall, Fe_3O_4 – opposite fire wall, Fe_2O_3 – fire wall, Fe_3O_4 – fire wall, respectively. One cycle consisted of polishing the layer to the depth of 2 µm (Fe_2O_3 – opposite fire wall), 5 µm (Fe_3O_4 – opposite fire wall), 5 µm (Fe_2O_3 – fire wall), 10 µm (Fe_3O_4 – fire wall). The exemplary of examine of XRD measurements has been shown in Figure 5.

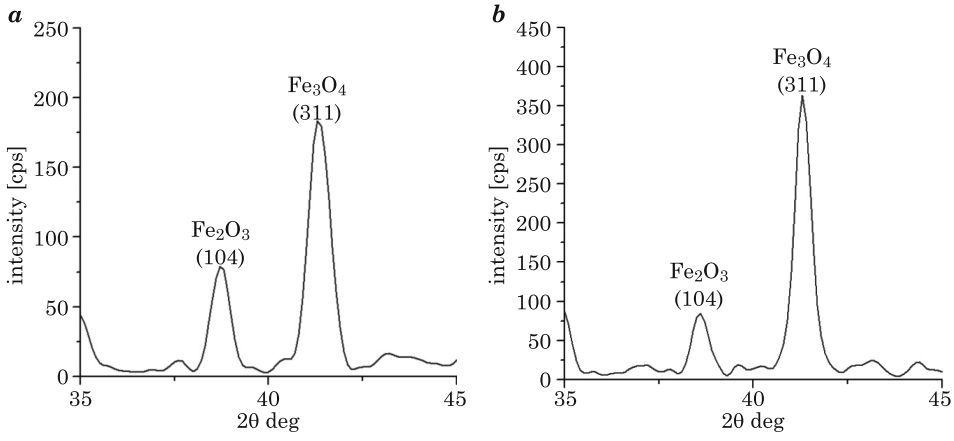

Fig. 5. X-ray diffraction patterns from the oxides layer obtained by means of XRD technique, after polishing: *a* – opposite fire wall, *b* – fire wall

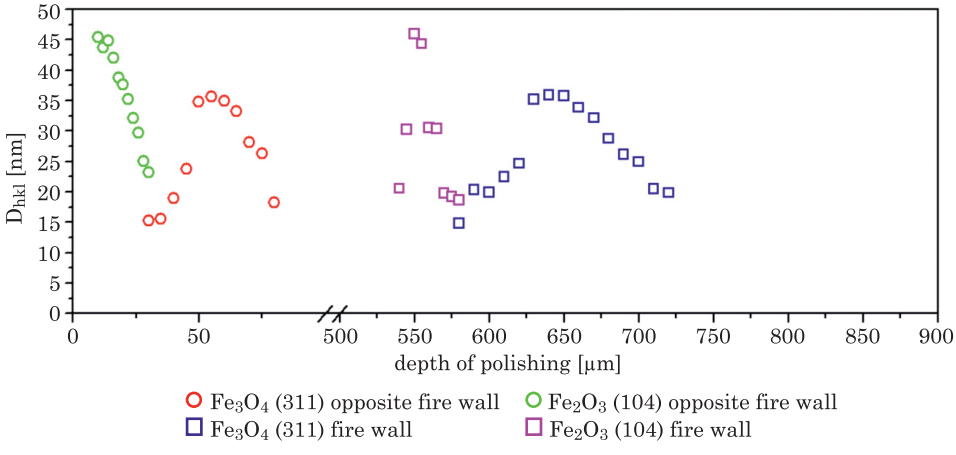

Fig. 6. Determination of crystallite size D_{hkl}

For the counter-fire side the size of hematite crystallites shows a downward trend after the next removal of the layer (Fig. 6). Fe_2O_3 crystallites at the depth of 10 μm are 45 nm in size. Instead, on the fire side the hematite peaks occur at the depth of 540 μm (Fig. 6). At this depth crystallites are 20 nm in size. A consecutive removal of the layer shows crystallites larger by 10 units, and the next two already by 15 units larger than in the previous polishing. At the depth of 560 μm the crystallites size is 30 nm. Instead, at the depth of 570–580 μm it is less than 20 nm. For magnetite in both cases (on the counter-fire as well as on the fire side) the crystallites size has a similar nature reaching the maximum of 35 nm (Fig. 6).

Summary

The paper contains assessment of hematite (Fe_2O_3) and magnetite (Fe_3O_4) formed on 10CrMo9-10 steel operated at the temperature of 525°C during 200,000 hours on the tube wall outside. Studies were carried out both for the fire and the counter-fire side. The obtained results of studies have shown that directly on the flue gas inflow side deposits are formed based on Al, Si and Ca. According paper (GAWRON, DANISZ 2012, GWOŹDZIK 2013) it has been found Al_2SiO_5 and $CaCO_3$.

The surface of deposits/oxides layer is more developed on the fire side. The deposits layer on the fire side is 539 μm thick, while on the counter-fire side only 10 μm. In both cases iron oxides Fe_2O_3 and Fe_3O_4 exist under the deposits layer. The size of hematite crystallites on the fire side at the maximum of its occurrence is D_{hkl} = 47 nm, while for the counter-fire side it is smaller by 2 units. Magnetite crystallites are smaller than those of hematite and in both cases (fire and counter-fire side) their size oscillates around 35 nm. The paper (GWOŹDZIK 2016) presents results of studies on oxides formed on the 10CrMo9-10 steel (on the flowing medium side (inside tube wall). Examinations carried out have shown that the formed layer is thicker and more degraded on the fire side. The size of crystallites on the fire side shows much larger dimensions both for hematite and magnetite. Instead, comparing the size of hematite and magnetite crystallites it is possible to state that in both cases (fire and counter-fire side) D_{hkl} is larger for hematite.

References

ANTONOV M., VEINTHAL R., HUTTUNEN-SAARIVIRTA E., HUSSAINOVA I., VALLIKIVI A., LELEIS M., PRISS J. 2013. *Effect of oxidation on erosive wear behaviour of boiler steels.* Tribology International, 68: 35–44.

BISCHOFF J., MOTTA A.T., EICHFELD C., COMSTOCK R.J., CAO G., ALLEN T.R. 2013. *Corrosion of ferritic-martensitic steels in steam and supercritical water*. Journal of Nuclear Materials, 441: 604–611.

FRANGINI S., MASCI A., MCPHAIL S.J., SOCCIO T., ZAZA F. 2014. *Degradation behavior of a commercial 13Cr ferritic stainless steel (SS405) exposed to an ambient air atmosphere for IT-SOFC interconnect applications.* Materials Chemistry and Physics, 144: 491–497.

GAWRON P., DANISZ S. 2012. *Dostosowanie zakresu badań diagnostycznych wybranych elementów kotłów pracujących w warunkach współspalania biomasy*. Energetyka, 702(12): 843–853.

GWOŹDZIK M. 2013. *Utlenianie stali 10CrMo9-10 podczas eksploatacji w wysokiej temperaturze*. Inżynieria Powierzchni, 1: 36–39.

GWOŹDZIK M. 2014. *Mechanizm degradacji warstw tlenkowych na stalach długotrwale eksploatowanych w energetyce.* Monografia, 291, Wydawnictwo Politechniki Częstochowskiej.

GWOŹDZIK M. 2016. *Analysis of Crystallite Size Changes in an Oxide Layer Formed on Steel Used in the Power Industry*. Acta Physica Polonica A, 130(4): 935–938.

KLEPACKI F., WYWROT D. 2010. *Trwałość wężownic przegrzewaczy wtórnych w warunkach niskoemisyjnego spalania*. Energetyka, 678(12): 816–820.

KLEPACKI F. 2006. *Korozja wysokotemperaturowa wężownic przegrzewaczy kotłów*. Energetyka, 621(3): 197–200.

KULESZA S., BRAMOWICZ M. 2014. *A comparative study of correlation methods for determination of fractal parameters in surface characterization*. Applied Surface Science, 293: 196–201.

LABISZ K. 2014. *Microstructure and mechanical properties of high power diode laser (HPDL) treated cast aluminium alloys*. Mat.-wiss. U. Werkstofftech, 45(4): 314–324.

LABISZ K. 2015. *Influence of Laser Feeding on Structure and Properties of Cast Aluminium Alloy Surface*. In: *Mechanical and Materials Engineering of Modern Structure and Component Design*. Eds. A. Öchsner, H. Altenbach. Advanced Structured Materials, 70. Springer, Cham, p. 317–343.

PRISS J., ROJACZ H., KLEVTSOV I., DEDOV A., WINKELMANN H., BADISCH E. 2014. *High temperature corrosion of boiler steels in hydrochloric atmosphere under oil shale ashes*. Corrosion Science, 82: 36–44.

SZAFARSKA M., IWASZKO J. 2012. *Laser remelting treatment of plasma-sprayed Cr_2O_3 oxide coatings*. Archives of Metallurgy and Materials, 57(1): 215–221.

ŢĂLU Ş., BRAMOWICZ M., KULESZA S., SHAFIEKHANI A., GHADERI A., MASHAYEKHI F., SOLAYMANI S. 2015. *Microstructure and Tribological Properties of FeNPs@a-C:H Films by Micromorphology Analysis and Fractal Geometry*. Industrial & Engineering Chemistry Research, 33 (54): 8212–8218.